Powder Technology 317 (2017) 301–309

Contents lists available at ScienceDirect

Powder Technology

journal homepage: www.elsevier.com/locate/powtec

Mixture and motion of sugar cane bagasse in a rotating drum

Érika Fernanda Rezendes Tada [a,*], Lina Maria Grajales [b], Yuri Pessoa Lemos [a], João Cláudio Thoméo [a]

[a] Departamento de Engenharia e Tecnologia de Alimentos, Instituto de Biociências, Letras e Ciências Exatas, Universidade Estadual de São Paulo (UNESP), Cristóvão Colombo 2265, Jardim Nazareth, 15054-000 São José do Rio Preto, SP, Brazil
[b] Departamento de Engenharia de Alimentos, Universidade Federal do Tocantins, Palmas – TO, Brazil, Quadra 109 Norte Avenida NS 15, 77001-090 Palmas, TO, Brazil

ARTICLE INFO

Article history:
Received 10 January 2017
Received in revised form 21 March 2017
Accepted 5 May 2017
Available online 7 May 2017

Keywords:
Rotating drum
Mixture and motion
Sugarcane bagasse
Image analysis
Tracer technique

ABSTRACT

The mixture and motion of fibrous particles of sugar cane bagasse were experimentally investigated in a rotating drum, a configuration frequently used for bioreactors in solid-state fermentation processes. The rotational velocity, filling degree and presence of an inner tube amidst the particles were the controlled variables. The image analysis technique was used to evaluate the radial and axial mixtures. The numbers of rotations used to achieve radial and axial homogeneities were obtained and the radial particle motion described. The minimum numbers of rotations for radial homogeneity were 12, 15 and 17 for filling degrees of 0.3, 0.5 and 0.6, respectively and this number was not influenced by the presence of the inner tube and the rotation velocity. The radial motion was influenced by all the variables and the flow regimes observed were distinct from those previously described in the literature. The passive layer did not behave as a solid body under any of the experimental conditions tested in the absence of the inner tube. When the tube was inserted, stagnant and fast velocities were observed in its vicinity and a porosity profile was noted in the stagnant zone. For both configurations, agglomerates of particles flowed down the free surface rather than a steady flow of particles. The axial diffusion coefficient was experimentally obtained and the simulated tracer concentration presented good agreement with the experimental results.

1. Introduction

Horizontal rotating drums partially filled with particles are often applied in industry (e.g., chemical, metallurgical, biotechnological, food), since the bed motion promotes high rates of heat and mass transfer amongst the particles, the drum wall and the surrounding gas. In order to build realistic heat and mass transfer models, knowledge of the flow patterns of the particles is mandatory.

Mellmann [1] characterized the flow regime of particles in rotating drums based on the filling degree (f_d) and on the Froude number (*Fr*). Of the proposed flow regimes, the cascade one is usually applied in industry, since there is enough shear stress between the drum wall and the particles to maintain steady particle circulation. This regime is divided into the sub-regimes of slumping, rolling and cascading. Under the rolling regime, the most common in industrial applications, [2] and [3], the particles are divided in two well-characterized regions: the active layer, where the particles continually move down the free surface of the bed, and the passive layer, in which the particles move as a solid body.

The studies on particle motion in rotating drums used either particles of conventional shapes, such as spheres and cylinders [1,4,5] and [6], or non-conventional shapes, such as rice [7] and [8], gravel, sand and limestone [9,10,11,12] and [13], lab made particles of different shapes [14], shale [12], tablets of several formats [15] and wood chips [16]. However, the dynamics of the movement of fibrous particles in rotating drums is little known. Some works attempted to foresee the movement of fibers using the Discrete Element Method [17] and [18], but only for low filling degrees, and only the work of Geng et al. [18] presented some experimental results for continuous axial flow on a bed of cut-tobacco, in order to determine the distribution of the particle residence time within the drum.

In solid-state fermentation (SSF), rotating drums are used to synthesize several high added-value products from solid wastes, generally with high filling degrees [19,20,21,22] and [23]. Sugar cane bagasse (SCB) has been processed in rotating drums to produce cellulases and hemicellulases required for second-generation ethanol production [24,25] and [26], and Grajales [27] used a rotating drum for such a purpose with promising results.

Of the techniques used to evaluate particle motion and mixture in rotating drums, Digital Image Processing (DIP) is widely applied [8,12,28,29] and [30] due to its simplicity and low cost. This technique often makes use of colored tracers and allows for the identification of segregation zones, flow regimes, active layer characteristics and velocity profiles.

This work aimed to investigate the mixture and movement of SCB fibers in a rotating drum in a batch process using DIP, the variables being the filling degree (f_d), the angular velocity (N) and the presence of an

* Corresponding author.
E-mail address: erikartada@gmail.com (É.F.R. Tada).

http://dx.doi.org/10.1016/j.powtec.2017.05.006
0032-5910/

inner tube. The transversal motion of the particles was described in detail, since no reports of particle movement of this nature were found in the literature. The results obtained will be employed as the basis for new studies involving irregular, fibrous and elastic particles, and the observations will be useful for modeling the motion of SCB in rotating drums as the basis for heat and mass transfer models.

2. Materials and methods

2.1. Particles and bed

The SCB was kindly provided by the *Usina Colombo*, Ariranha – SP, Brazil, an ethanol and sugar producing industry. The bagasse was donated with 50% moisture content (w.b.), and was moistened to 75% for the experiments, since this is the typical moisture content required by the SSF process for enzyme production [27,31] and [32]. Particles visually larger than the average were manually removed from the bagasse and part of the material was dyed with a 0.02% (w/v) solution of Rodamine B to produce a colored tracer.

The mass of moist SCB fibers varied between 3 kg and 6 kg. Table 1 presents the mean sizing of the SCB fibers and the physical properties of the particle bed used in this study. The SCB was assumed to be in the form of infinite cylinders throughout the study.

2.2. Experimental apparatus

The experiments were carried out in an acrylic drum, with an inner diameter of 30 cm and length of 60 cm, as shown in Fig. 1. The drum had four internal 3 cm wide lifters at an angle of 45° to the drum wall. Some experiments were carried out inserting an inner tube longitudinally amidst the bed of particles, as shown in Fig. 1. This acrylic tube remained static during the experiments and aimed to simulate the presence of the tube used to supply air to the cultivation medium in a SSF bioreactor. The front and back lids remained stationary during the experiments, such that only the drum wall rotated. The drum was sustained by a metallic structure, which provided angular rotation at controlled velocities. All experiments were carried out in the batch mode.

2.3. Calibration of the software for the image analysis

The software LensEye (Engineering & Cyber Solutions, Gainesville, USA) was used for the DIP and required calibration. Following the recommendations of Grajales and co-workers [8], the software was adjusted to identify areas with the characteristic color of Rodamine B. The calibration was done with 15 g samples of bagasse, with mass concentrations of dyed particles varying from 0 to 100%. The samples were placed in Petri dishes and photographs taken under controlled illumination using a DCR-DVD408 digital camera (Sony *Co*., Tokyo, Japan). The images were processed by the software as a percentage of the dyed area. Fig. 2 presents photographs of samples prepared in Petri dishes with different concentrations of dyed area.

2.4. Mixing experiments

The experiments were carried out with the filling degrees and rotation velocities shown in Table 1. The filling degree is the ratio between the transversal area occupied by the particles and the total transversal area of the drum, as follows:

$$f_d = \frac{\varepsilon - \cos(\varepsilon) \cdot \sin(\varepsilon)}{\pi} \quad (1)$$

where the angle ε is shown in Fig. 3.

Three particle loads were used (3.0, 4.5 and 6.0 kg). Each load was individually placed within the drum and rotated up to the moment that the dynamic repose angle (θ) was observed to be constant. At this moment, the front lid was photographed and the angle ε determined.

The mass of dyed particles was fixed at 30% of the total mass of particles in each experiment, following the results of the software calibration. The initial positions of the particles for the radial and axial mixture experiments are shown in Fig. 4.

The majority of the experiments followed a full statistical factorial design of random blocks at three levels. The independent variables were f_d and N, and the levels are shown in Table 2. The response variables were the number of rotations required to achieve radial and axial homogeneity (N_{rad} and N_{ax}, respectively) and the axial dispersion coefficient (D_z). As can be seen in the Results and Discussion section, the presence of the inner tube did not affect the response variables and thus this factor was not included in the design. The statistical analyses were carried out using the Minitab 16.2 (Minitab Inc., State College, USA) at a 95% confidence level, except when stated otherwise.

For the radial mixture experiments, the selected particle load was inserted into the drum, which was then rotated at the selected rotation velocity. Under controlled illumination, the front lid was recorded using the DCR-DVD408 digital camera for 30 min. The video was analyzed using the *Picture Motion Broswer* software (Sony *Co*., Tokyo, Japan) and the selected images analyzed using the LensEye software to determine the tracer concentration. The mixture was considered homogeneous when the dyed area identified by the LensEye software was equal to 30% ± 2%.

For the axial mixture analysis, the drum was virtually divided into five axial regions. At consecutive 15 min intervals, the drum rotation was halted and the bed surface photographed with the DCR-DVD408 camera (Sony *Co*., Tokyo, Japan) under controlled illumination. The images were analyzed using the LensEye software using the same criterion for homogeneity as used for the radial mixture.

2.5. Transverse motion experiments

The videos acquired during the radial mixture experiments were also used to qualitatively evaluate the particle motion. The flow regimes observed were compared with those described by Mellmann [1], according to the filling degree and the Froude number, defined by:

$$Fr = \frac{(2\pi\ N)^2 R}{g} \quad (2)$$

where R is the drum radius and g is the gravity acceleration.

Table 1
Sizing of the SCB fibers and the physical properties of the particle bed.

Symbol	Parameter	Value	Method
d_p	Mean diameter	0.065 cm ± 0.014 cm	Direct measurement of ten fibers at random
L_p	Mean length	1.07 cm ± 0.25 cm	
v_p	Mean volume	3.55×10^{-3} cm^3	Approximate geometry to an infinite cylinder
ρ_{bulk}	Bulk density of the bed	0.21 g cm^{-3} ± 0.02 g cm^{-3}	Ratio between the mass of particles and the volume occupied in the drum
α	Bed porosity	0.75 (−)	[32]

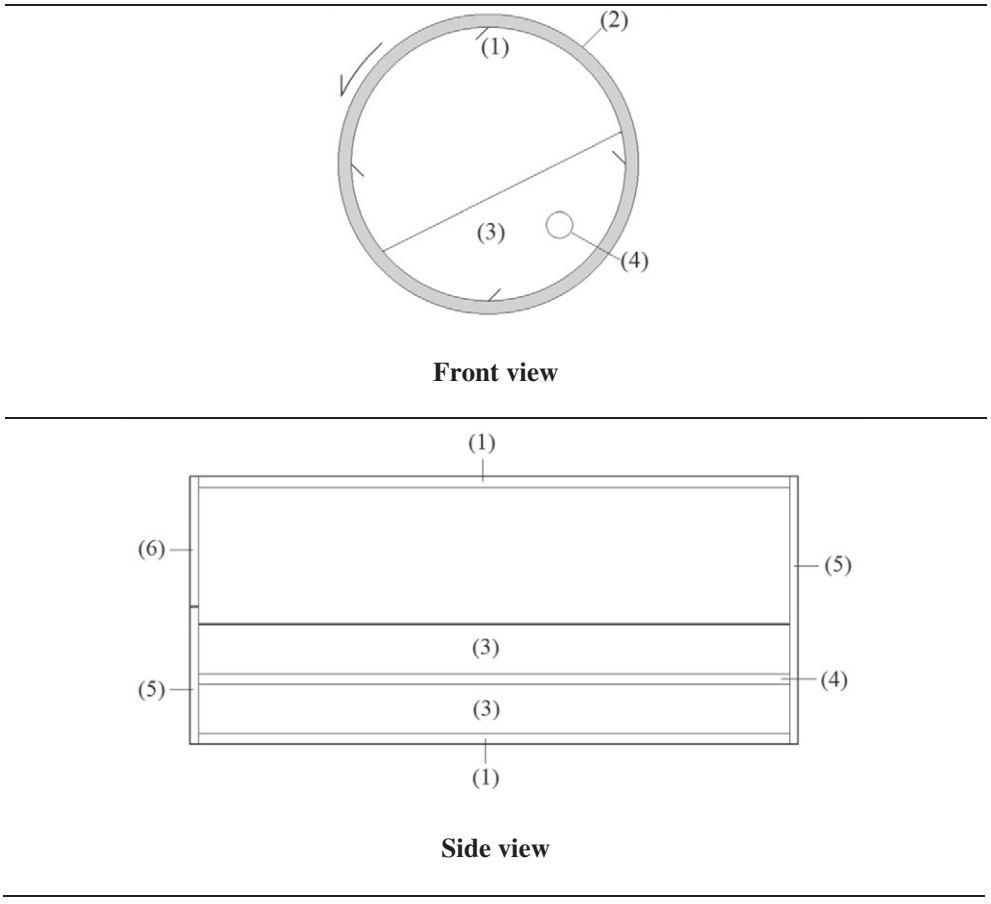

Fig. 1. Sketch of the drum, presenting details of the inner tube and internal lifters, positioned at 45° to the drum-wall. (1) – lifter, (2) – drum wall, (3) – bed of fibers, (4) – inner tube, (5) – stationary lids, (6) – loading window.

2.6. Determination of the axial dispersion coefficient (D_z)

The axial dispersion coefficient was determined from the solution of the diffusion equation applied to the longitudinal axis, as follows:

$$\frac{\partial C}{\partial t} = D_z \frac{\partial^2 C}{\partial z^2} \tag{3}$$

where C is the tracer concentration, t is the variable time and z is the axial coordinate.

The required boundary and initial conditions to solve Eq. (3) are:

$$t = 0 \qquad z < L, \qquad C = C_0 \tag{4}$$

$$t = 0 \qquad z \geq L \qquad C = 0 \tag{5}$$

$$z = 0 \qquad \frac{\partial C}{\partial z} = 0 \tag{6}$$

$$z = L \qquad \frac{\partial C}{\partial z} = 0 \tag{7}$$

The integration of Eq. (3) results in [33]:

$$\frac{C}{C_0} = \frac{L^*}{L} + \frac{2}{\pi} \sum_{n=1}^{\infty} \frac{1}{n} sen\left(\frac{n\pi L^*}{L}\right) \cos\left(\frac{n\pi z}{L}\right) \exp\left(-\frac{n^2\pi^2}{L^2} D_z \ t\right) \tag{8}$$

where C_0 is the initial tracer concentration; L is the total drum length; and L^* is the drum length occupied by the dyed particles. To estimate the values for D_z, the values of $C = C(z)$ were obtained experimentally using the image analysis method.

From the estimated values obtained for D_z, the axial concentrations of dyed particles were simulated using Eq. (3). A program in MatLab® R2012b (MathWorks Inc., Natick, USA) language was developed, and the partial differential equation was discretized by the finite difference method. The resulting ordinary differential equations were solved using the ode45 solver.

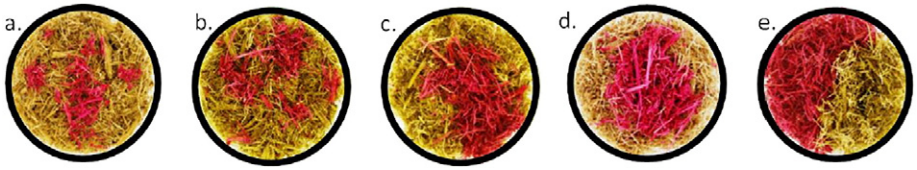

Fig. 2. Samples of SCB particles prepared with (a) 5%, (b) 10%, (c) 20%, (d) 30% and (e) 60% of dyed area.

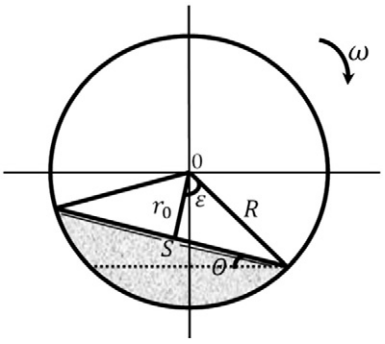

Fig. 3. Sketch of the front view of the partially filled drum.

3. Results and discussion

3.1. Software calibration

Fig. 5 presents the experimental data obtained in the calibration of the LensEye software. Good linearity was observed between the tracer concentrations and the areas identified by the software, and the linear regression resulted in a high determination coefficient ($R^2 = 0.996$) and an almost unitary angular coefficient (1.03). Significant errors were only observed for tracer concentrations under 10%. Therefore a tracer concentration of 30% was chosen for the subsequent experiments.

3.2. Dynamic repose angle (θ)

The average values observed for θ with and without the inner tube were 32.2° ± 5.8° and 37.7° ± 7.1°, respectively. Generally, the presence of the inner tube resulted in a lower repose angle and only for the higher f_d (0.6) value was this trend not observed. Nevertheless, the variables f_d and N did not present a definite influence on θ.

Grajales and co-workers [8] carried out experiments using the same drum and observed average values for θ equal to 42.6° for moist rice, 22.7° for glass beads of 3 mm in diameter and 25.0° for silica gel beads of 6 mm in diameter. Dubé and co-workers [15] presented values for θ which ranged from 29.27° to 32.34° for particles showing several different shapes and sizes. Henein and co-workers [9] used a variety of particles (gravel, iron oxide, limestone, nickel oxide and sand), with particle diameters (d_p) ranging from 0.23 to 11.6 mm and found values for θ ranging from 30.2° to 41.5°. The authors did not find a defined trend for θ with N and f_d, but found a well-defined dependence of θ on the shape of the particles, resulting in lower values for θ for spherical and granular particles and higher values for irregular particles. Hence the values for θ for particles of SCB were in the range observed for irregular particles, even though the shape and the elasticity of the SCB particles were quite different from those found in the reported literature.

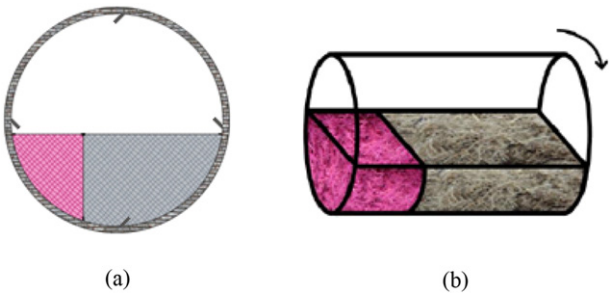

Fig. 4. Initial positions of the particles for the radial (a) and axial (b) mixture experiments.

Table 2
Selected independent variables and their respective levels for the full statistical design of the mixture experiments.

Variables	Levels		
	−1	0	1
N (rpm)	1	4	7
f_d (−)	0.4	0.5	0.6

3.3. Radial mixture

Table 3 presents the results for the minimum number of rotations required to achieve radial homogeneity (N_{rad}), where it can be seen that the rotational velocity did not influence N_{rad}. For the filling degrees of 0.4, 0.5 and 0.6 the values for N_{rad} were 12, 15 and 17, respectively. Although the quantity of f_d was reduced, a linear trend was noticed between N_{rad} and f_d ($R^2 = 0.993$), resulting in the following equation:

$$N_{rad} = 2.2 + 25\ f_d \tag{9}$$

Kwapinska and co-workers [34] used DEM to simulate the transverse mixing of spherical particles, with d_p values ranging from 2.5 to 3.4 mm, N from 9.1 to 19.1 rpm and f_d equal to 20 and 30%. The authors found that the depth of the active layer increased with the increase in f_d, improving the radial mixture. Nevertheless, an increase in f_d increased the depth of the passive layer even more, resulting in an increase in N_{rad}. Van Puyvelde and co-workers [12] studied the transversal motion of shale in the rolling regime and proposed a correlation for the ratio between the depth of the active layer and the depth of the passive layer (%AL), as follows:

$$\%AL = 9.81\ \ln(N) + 0.438e^{[0.08744(50-f_d)]} \tag{10}$$

where the %AL is given in percentage.

Applying Eq. (10) to the experimental conditions of this work, %AL ranged from 0.2 to 20.1%. This ratio was dependent on N, but not on f_d, at a 95% significance level. Eq. (10) was validated by [12] using the experimental data of [28] for shale particles with the d_p varying from 0.89 to 5.08 mm, rotational velocity from 5.17 to 15.10 rpm and f_d from 10 to 40%. The resulting values for %AL of van Puyvelde and co-workers [12] varied from 16 to 41%. Therefore, even though the particles of the present study were quite different from those of shale, the proportion calculated for %AL was small enough to justify the large number

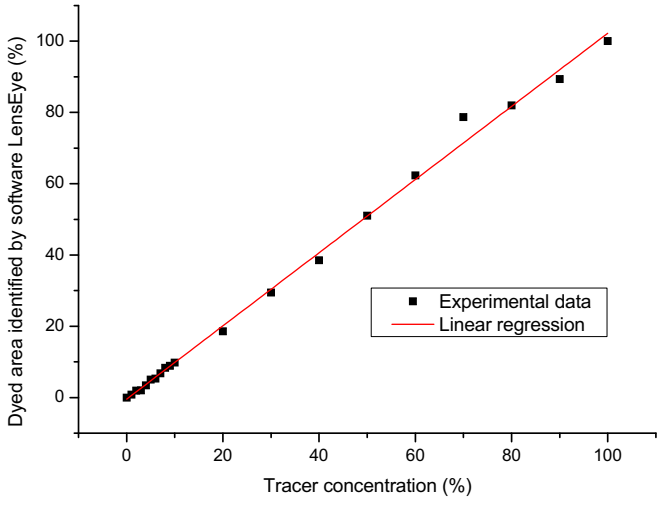

Fig. 5. Areas identified by the LensEye software obtained from the tracer concentrations in the SCB dyed with Rodamine B.

Table 3
Tracer concentration for the experiments of radial mixture given in % of tracer, with a homogeneity criterion of 30% of tracer.

f_d (−)	Inner tube	N (rpm)	10^{-3} *Fr* (−)	N_{rad} (revolutions)		
				12	15	17
0.4	With	1	0.2	29.8	–	–
		4	2.7	31.5	–	–
		7	8.2	29.4	–	–
	Without	1	0.2	30.7	–	–
		4	2.7	31.7	–	–
		7	8.2	29.8	–	–
0.5	With	1	0.2	46.3	31.0	–
		4	2.7	51.0	31.8	–
		7	8.2	48.7	29.4	–
	Without	1	0.2	52.1	31.5	–
		4	2.7	39.4	29.8	–
		7	8.2	45.6	29.9	–
0.6	With	1	0.2	–	45.8	32.0
		4	2.7	–	51.6	30.5
		7	8.2	–	46.5	31.8
	Without	1	0.2	–	53.8	30.4
		4	2.7	–	40.1	31.4
		7	8.2	–	46.8	31.7

observed for N_{rad}, and, as will be seen below, it also had an influence on the axial mixture.

Schlünder and Mollekopf [35] proposed a correlation for N_{rad} for drum dryers operating with regular shaped particles under vacuum. The correlation was based on the penetration theory, and aimed to obtain a uniform temperature profile within the bed, showing that N_{rad} was only dependent on the Froude number, as follows:

$$N_{rad} = 16\ Fr^{0.2} \tag{11}$$

Applying Eq. (11) to the experimental conditions of the present work resulted in values for N_{rad} lower than those obtained experimentally, indicating that the proposed model was limited to the kind of particles employed here.

Schutyser [36] mixed moist wheat grains in a drum with a diameter of 30 cm and length of 40 cm and observed homogeneous mixtures after 4 and 8 rotations for f_d equal to 0.33 and 0.40, respectively. Grajales and co-workers [8] used a drum similar to that applied here and obtained homogeneous mixtures after 5, 9 and 11 rotations for f_d equal to 0.23, 0.33 and 0.40, respectively. Therefore, the values for N_{rad} determined here were higher than those observed in the literature, indicating that the nature of the particles, elastic and interlacing, were responsible for the resistance to the mixture, since part of the rotational energy supplied by the drum to the bed is indeed used to deform the fibers and not to move them.

3.4. Transverse motion

The transverse particle motion was steady and orderly in every region of the bed for the experiments without the inner tube. To the contrary, for the experiments with the inner tube, regions with different velocities were observed in the passive layer. Since the number of rotations required to obtain radial homogeneity (N_{rad}) was not affected by the presence of the inner tube, this may infer that the poor particle circulation was compensated by higher velocities in other regions in the passive layer when the inner tube was inserted, which cannot be considered as a solid body anymore. Grajales and co-workers [8] observed similar behavior in experiments using rice in a bed with a submerged tube.

Mellmann [1] proposed a flow regime classification based on both the Froude number and the filling degree. If this classification was applied to the range of *Fr* and f_d used in this work, the flow regime *Slipping* with the sub-regime *Surging*, and the regime *Cascading* with the sub regime *Rolling*, would be determined. However, the movements observed were atypical in the active layer, with and without the inner tube. The typical formation of wedges for the sub-regime *Surging*, or the continual flow of particles for the sub-regime rolling, were not noted. For particles usually tested in rotating drums (e.g., sugar, gravel, limestone and sand), the action of the lifters did not affect strongly the active and the passive layers, even though Grajales and co-workers [8] noticed that the lifters caused a certain intermittence to the flow of the active layer. In the current study, the lifters carried an expressive amount of particles, which were thrown against the active layer in definite positions. Simultaneously, portions of particles between two adjacent lifters acquired enough potential energy to flow down the slope. Nevertheless, due to the interlacing of the fibers, the flow of particles took place in blocks. Therefore, these two contributions caused a flow of blocks of irregular shapes, velocities and frequencies, and the flow regimes suggested by Mellmann [1] were not valid for flexible, interlacing and irregular fibers.

To improve the understanding of the transverse particle motion for the experiments without the inner tube, Fig. 6 represents an experiment for f_d equal to 0.5 and N equal to 1 rpm. When the bed surface was between two consecutive lifters (Fig. 6a), small blocks of particles tumbled down the free surface up to the opposite wall of the drum, in what could be called the active layer. Under such conditions, the passive layer was not visually affected by the movement of the particles on the active layer, behaving as a solid body. For the situation represented in Fig. 6b, larger blocks, coming from the upper lifter, were thrown against the active layer, and the passive layer was flexed, with some particles being displaced. The lifters also promoted some empty zones at the top of the free surface, as can be seem in Fig. 6c, interrupting the flow of the blocks of particles coming from the upper drum wall. Fig. 7 presents a

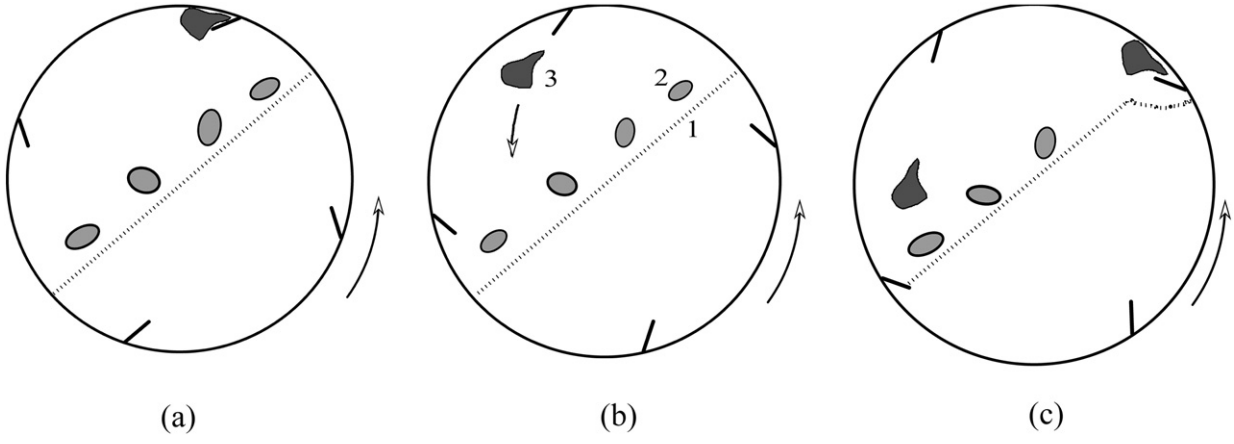

Fig. 6. Transverse view of the drum without the inner tube, showing the position of the lifters, for the rotation velocity of 1 rpm (1 - Bed surface; 2 - Small blocks; 3 - Large blocks).

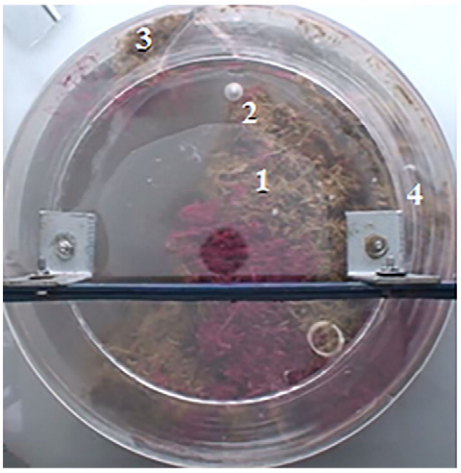

Fig. 7. Captured image during the experiments of transverse motion of SCB particles in rotary drum without inner tube, for filling degree 0.5 and rotational velocity of 1 rpm (1 – Large blocks, 2 – Small blocks, 3 – Portion of particles carried by lifters, 4 – Empty space below lifter).

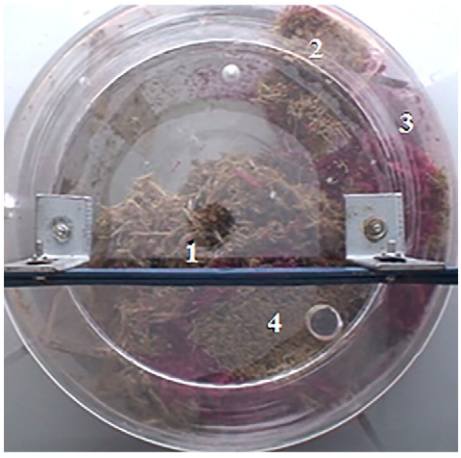

Fig. 9. Captured image during the transverse motion of SCB particles in rotary drum with inner tube, for filling degree 0.5 and rotation velocity of 1 rpm (1 – Large blocks, 2 – Portion of particles carried by lifters, 3 – Empty area below lifter, 4 – Stagnant zone nearby inner tube).

captures image during the experiments of transverse motion in absence of inner tube.

The filling degree did not drastically change the described flow pattern, but promoted some small modifications. For instance, for f_d equal to 0.4, the hollow space shown in Fig. 6c was larger and the fall of the large block from the upper lifter was higher, causing a more intense motion of particles in the passive layer. For f_d equal to 0.6, the large block did not fall at once, but fell down in smaller blocks, although still larger than the ones coming from the drum wall, and the effect of these falls on the passive layer was not so intense. For the higher rotational velocities, the particle motion became more irregular and difficult to characterize.

For the experiments with the inner tube, a similar behavior was observed for the active layer to that in the experiments without the tube. Nevertheless, the inner tube caused a stagnant zone and a fast velocity zone in the passive layer, as represented in Fig. 8. In the stagnant zone, particle compression was observed causing a reduction in porosity. On the opposite side of the tube, the high velocity of the particles fluidized the bed, reducing its porosity. Since the purpose of the inner tube is to supply air to the microbial cultivation in a SSF bioreactor, when the bed is halted after being rotated, irregular bed porosity will be found and the air velocity profile will be complex. It must be pointed out that microbial cultivation in the drum usually takes place under stationary conditions in order to avoid damage to the microbial physiology, and drum rotation is used only occasionally to homogenize the temperature and water concentration profiles. Fig. 9 presents a real image captured during the tests of transverse motion of SCB particles with inner tube, in which is possible to visualize the behavior noticed.

The stagnant zone shown in Fig. 8 was deformed according to the positions of the lifters. When the large blocks were thrown against the active layer (Fig. 6b), some particles in the stagnant zone were displaced and particles from the outskirts replaced them. An increase in the filling degree increased the size of the stagnant zone but also of the fast velocity zone; and consequently, the overall flow rate of the particles in the passive zone was not affected by the presence of the inner tube and N_{rad} was unchanged by its presence. An increase in the rotation velocity increased the particle movement for every filling degree. For f_d equal to 0.4 and N equal to 7 rpm, the stagnant zone was practically extinguished, and an intense motion of particles was observed in the so called passive region. The size of the stagnant zone was strongly affected by the falling of large blocks from the upper lifters.

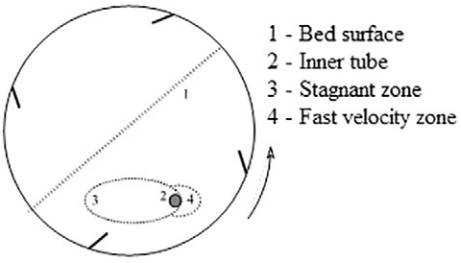

Fig. 8. Transverse view of the drum with the inner tube for $f_d = 0.5$ and $N = 1$ rpm.

3.5. Axial mixture

Fig. 10 presents the experimental data for the number of rotations required to achieve axial homogeneity (N_{ax}) as a function of f_d and N, as well as the surface response provided by the linear statistical model. The value for N_{ax} was up to 63 times higher than N_{rad}, since in batch experiments axial mixture only takes place by diffusion, which represents the random motion of particles in the active layer. Fig. 10 shows the linear trend of N_{ax} with f_d and N. It must be highlighted that the presence of the inner tube did not affect the value of N_{ax}, reinforcing the fact that the active layer was indeed similar, with and without the inner tube.

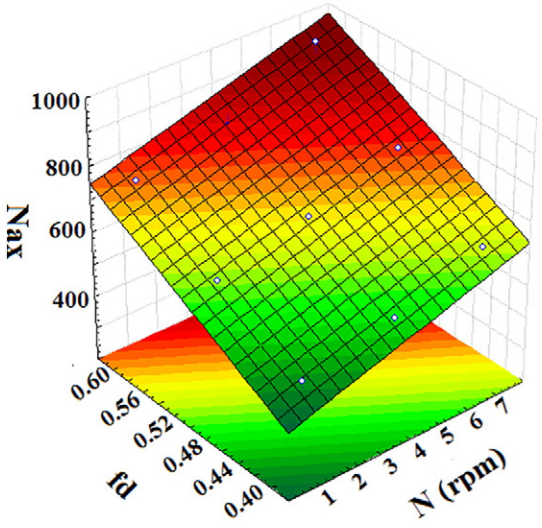

Fig. 10. Number of rotations required to achieve axial homogenization as a function of the filling degree and the rotational velocity, with the response surface provided by the linear statistical model (colored area – surface response; ○ – experimental data).

The linear statistical model, without the cross interaction term, presented a high determination coefficient ($R^2 = 0.986$), and the resulting equation to forecast N_{ax} is:

$$N_{ax} = -126.9 + 1408.3\ f_d + 28.1\ N \quad (12)$$

The coefficient of axial diffusion, calculated using Eq. (8), is presented in Fig. (11a) and (b). The linear statistical model resulted in a high determination coefficient ($R^2 = 0.95$) without the cross interaction coefficient, and the factor f_d was significant at the 90% confidence level. The resulting equation for D_z is:

$$D_z = 9.58 - 18.95\ f_d + 2.34\ N \quad (13)$$

Fig. (11a) presents the experimental data and the surface response for the statistical model, where one can see that an increase in f_d decreased D_z. According to the literature, D_z should decrease logarithmically ([37] – particles of Na_2CO_3 and $NaHCO_3$), with the square root ([7] – rice; [6] – glass beads), or irregularly ([29]- DEM simulation using spherical particles) with f_d, for the flow regimes of slumping, rolling and cascading. In fact, if D_z is only represented as a function of f_d (Fig. 11b), the observed trend for the decay of D_z is not linear for the highest rotational velocities (4 and 7 rpm). Nevertheless, if the quadratic term related to f_d is introduced into the statistical model, it would only be significant at the 75% significance level. Therefore, only new experiments at different filling degrees could provide a better understanding of the decay of D_z with f_d. As previously discussed, the ratio between the depth of the active layer and the depth of the passive layer (%AL) decreases with an increase in f_d, resulting in a reduction in D_z.

The values for D_z obtained here were in the same range as those found in the literature [7,6] and [15]. Sherritt and co-workers [6] proposed an equation to represent 179 experimental data found so far in the literature, and represented as follows:

$$D_z = k\left(\frac{N}{N_c}\right)^c (2R)^b d_p^c (f_d)^d \quad (14)$$

where N_c is the critical rotational velocity (rpm); and a, b, c, d and k are constants which depend on N/N_c and on the flow regime. The factor N_c is the rotational velocity above which the bed motion is dominated by the centrifugal field, and was given by:

$$N_c = \frac{60}{2\pi}\sqrt{\frac{g}{R}} \quad (15)$$

Table 4
Axial dispersion coefficients calculated using Eq. (14) and the experimental values obtained in this work as a function of the filling degree and the rotational velocity.

f_d (−)	N (rpm)	D_z (m^2/s)	
		Experimental	Sherrit et al. (2003)
0.4	1	$4.03\cdot10^{-6}$	$7.73\cdot10^{-6}$
	4	$2.19\cdot10^{-5}$	$1.46\cdot10^{-5}$
	7	$3.31\cdot10^{-5}$	$1.89\cdot10^{-5}$
0.5	1	$3.30\cdot10^{-6}$	$7.03\cdot10^{-6}$
	4	$1.54\cdot10^{-5}$	$1.33\cdot10^{-5}$
	7	$2.43\cdot10^{-5}$	$1.72\cdot10^{-5}$
0.6	1	$2.73\cdot10^{-6}$	$6.50\cdot10^{-6}$
	4	$1.44\cdot10^{-5}$	$1.23\cdot10^{-5}$
	7	$2.30\cdot10^{-5}$	$1.59\cdot10^{-5}$

The range of D_z used to produce Eq. (14) varied from 10^{-7} to 10^{-4} m^2/s, and comprehended all the regimes usually found in the literature [6]. Table 4 presents values for D_z estimated using Eq. (14) and the values obtained experimentally, where one can see that the experimental and estimated values were of the same order of magnitude, with deviations similar to those observed by [6]. Hence, even though the particles here applied and the flow regime observed were different from those found in the literature, the axial diffusive motion was similar to the other systems. For the calculation of d_p, as required by Eq. (14), it was used the value of a sphere of equivalent diameter to the volume of the real particles. The volume of the particles was calculated assuming them as infinite cylinders with the dimensions presented in Table 1. The flow regimes were assumed to be similar to those reported by [1] and were determined for the values of *Fr* and f_d used in this work.

Fig. 12 presents the experimental values found for the tracer concentration in the longitudinal direction and the values calculated from the numerical solution of Eq. (3), using the values for D_z obtained here for f_d equal to 0.4 and N equal to 1 rpm, for the drum configuration without the inner tube. Good agreement can be seem between the experimental and calculated tracer concentrations, as also observed by [29] using a one-dimensional plug-flow model for a rotating drum with overall axial particle motion, although [30] presented some criticism of the results of those authors based on the Froude number.

3.6. Further studies about mixing and motion of organic particles and the application in solid-state fermentation process

This paper presented qualitative and quantitative approaches of the dynamics of movement of fibrous particles in a rotating drum. As mentioned above, this is the first step in the understanding of this

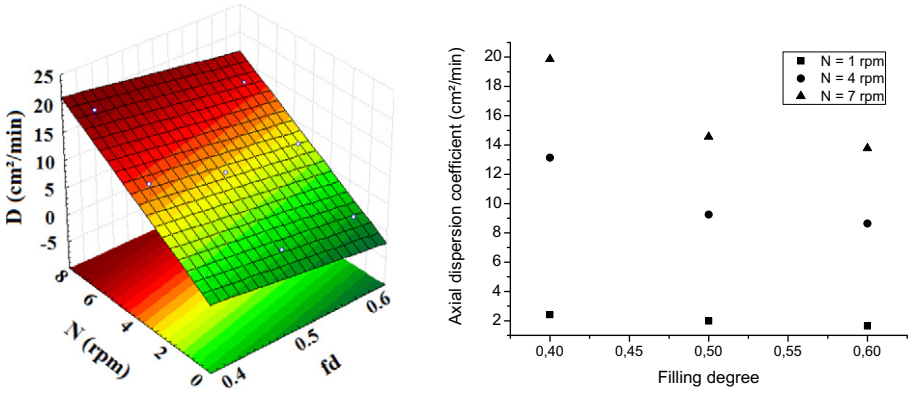

Fig. 11. Axial dispersion coefficient as a function of the filling degree and the rotational velocity: (a) surface response provided by the linear statistical model (colored area – surface response; ○ – experimental data); (b) Nonlinear dependence of D_z on the filling degree.

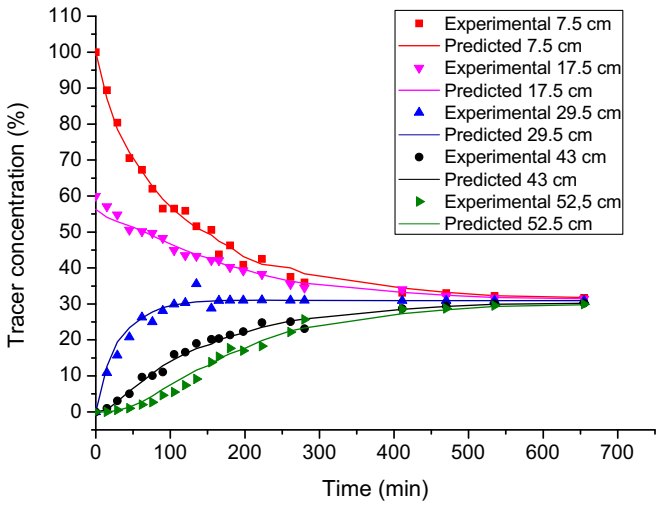

Fig. 12. Longitudinal tracer concentration simulated using the diffusional differential equation and values experimentally obtained for the filling degree of 0.4 and rotational velocity of 1 rpm, without the inner tube.

engineering aspect in rotating drums constructed for solid state fermentation. The next steps consist of the study of the dynamics of fibrous particles in the presence of mycelium, referring to the real fermentation situation. This study, pioneer in the use of such particles, did not contemplate the presence of an external structure on the particles, and one can imagine that such a structure could strongly influence the dynamics of movement during the process. In addition the particle bed in a reaction medium tends to accumulate heat, due to the metabolic activities of the microorganism, allowing for the installation of temperature and moisture gradients in the spatial domain, modifying the bed conditions during the process. Certainly the results observed here will be of great importance in the understanding of the dynamics of the particles in the presence of mycelium, and can be used as a basis for future studies of movement transport allied to heat and mass transport in partially filled horizontal drums during solid state fermentation processes.

4. Conclusions

The study of the mixture and motion of sugar cane bagasse particles in a rotating drum was reported in this paper. The process variables adopted were the rotational velocity, the filling degree and the presence of an internal tube axially disposed amongst the particles. Image analysis was successfully applied to determine the number of rotations required to obtain radial and axial homogeneities, which were only dependent on the filling degree. Radial motion was completely different from those reported in the literature for the active and the passive layers. The particle motion on the free surface was not steady and blocks of several sizes were observed, depending on the relative positions of the lifters and on the rotational velocity. The central core did not move as a solid body for any of the experimental conditions adopted. The presence of the inner tube affected the passive layer, and regions of very low and very fast velocities were observed. A variation in the porosity of the bed was also noticed in the case of using the inner tube. The axial dispersion coefficient was experimentally determined from the diffusion model and the simulated tracer concentration presented good agreement with the experimental results. The results here obtained will be of help for the modeling and operation of rotating dryers and bioreactors that use fibers as particulate system. The flexible nature of the fibers and their interlacing promote significant modifications in the pattern of particle movement known so far in the literature and one might expect difficulties in representing such movement adequately.

Nomenclature

%AL	Ratio between the depth of the active layer and the depth of the passive layer	%
C	Tracer concentration	Dyed area/total area
C_0	Initial tracer concentration	Dyed area/total area
d_p	Mean particle diameter	cm
D_z	Axial dispersion coefficient	cm^2/s
f_d	Filling degree	–
Fr	Froude number	Dimensionless
g	Gravity acceleration	$m\ s^{-2}$
L	Drum length	cm
L_p	Mean particle length	cm
L^*	Length of the drum occupied by dyed particles	cm
N	Rotational velocity	rpm
N_{ax}	Minimum number of rotations for axial homogeneity	–
N_c	Critical rotational velocity	rpm
N_{rad}	Minimum number of rotations for radial homogeneity	–
r_0	Distance between the bed surface and the rotation axis	m
R	Drum radius	m
S	Distance travelled by the particles on the solid bed	m
t	Time	s or min
v_p	Mean particle volume	cm^3
z	Axial position	cm
α	Bed porosity	cm^3 empty spaces/cm^3 total volume
ε	Static repose angle	° or radian
ρ_{bulk}	Bulk bed density	$g\ cm^{-3}$
θ	Dynamic repose angle	° or radian
ω	Angular velocity	$rad\ s^{-1}$

Acknowledgements

The authors are grateful to the sponsors of this work: The *Coordenação de Aperfeiçoamento de Pessoal de Nível Superior* (CAPES) (Social Demand ## 33004153070P-2) and The *Fundação de Amparo à Pesquisa do Estado de São Paulo* (FAPESP) (Processo ##2014/23453-3).

References

[1] J. Mellmann, The transverse motion of solids in rotating cylinders — forms of motion and transition behavior, Powder Technol. 118 (2001) 251–270.
[2] A.A. Boateng, B.V. Barr, Modelling of particle mixing and segregation in the transverse plane of a rotary kiln, Chem. Eng. Sci. 51 (1996) 4167–4181.
[3] A.A. Boateng, Rotary kilns: transport phenomena and transport process, first ed. Jordan Hill, Oxford, 2008.
[4] G. Félix, V. Falk, U. D'Ortona, Segregation of dry granular material in rotating drum: experimental study of the flowing zone thickness, Powder Technol. 128 (2002) 314–319.
[5] X.Y. Liu, E. Specht, J. Mellmann, Experimental study of the lower and upper angles of repose of granular materials in rotating drums, Powder Technol. 154 (2005) 125–131.
[6] R.G. Sherritt, J. Chaouki, A.K. Mehrotra, L.A. Behie, Axial dispersion in the three-dimensional mixing of particles in a rotating drum reactor, Chem. Eng. Sci. 58 (2003) 401–415.
[7] R. Rutgers, Longitudinal mixing of granular material flowing through a rotating cylinder: part II experimental, Chem. Eng. Sci. 20 (1965) 1089–1100.
[8] L.M. Grajales, N.M. Xavier, J.P. Henrique, J.C. Thoméo, Mixing and motion of rice particles in a rotating drum, Powder Technol. 222 (2012) 167–175.
[9] H. Henein, J.K. Brimacombe, A.P. Watkinson, Experimental study of transverse bed motion in rotary kilns, Metall. Trans. B 14 (1983) 191–205.
[10] H. Henein, J.K. Brimacombe, A.P. Watkinson, Experimental study of segregation in rotary kilns, Metall. Trans. B 16 (1985) 763–774.
[11] A.A. Boateng, P.V. Barr, Granular flow behavior in the transverse plane of a partially filled rotating cylinder, J. Fluid Mech. 330 (1997) 233–249.
[12] D.R. Van Puyvelde, B.R. Young, M.A. Wilson, S.J. Schmidt, Modeling transverse segregation of particulate solids in a rolling drum, Chem. Eng. Res. Des. 78 (2000) 643–650.
[13] A. Ingram, J.P.K. Seville, D.J. Parker, X. Fan, R.G. Forster, Axial and radial dispersion in rolling mode rotating drums, Powder Technol. 158 (2005) 76–91.
[14] G.R. Woodle, J.M. Munro, Particle motion and mixing in a rotary kiln, Powder Technol. 76 (1993) 241–245.
[15] O. Dubé, E. Alizadeh, J. Chaouki, F. Vertrand, Dynamics of non-spherical particles in a rotating drum, Chem. Eng. Sci. 101 (2013) 486–502.
[16] B. Colin, J.L. Dirion, P. Arlabosse, S. Salvador, Wood chips flow in a rotary kiln: experiments and modeling, Chem. Eng. Res. Des. 98 (2015) 179–187.
[17] F. Geng, Y. Li, X. Wang, Z. Yuan, Y. Yan, D. Luo, Simulation of dynamic processes on flexible filamentous particles in the transverse section of a rotary dryer and its comparison with ideo-imaging experiments, Powder Technol. 207 (2011) 175–182.

[18] F. Geng, Y. Li, L. Yuan, M. Liu, X. Wang, Z. Yuan, Y. Yan, D. Luo, Experimental study on the space time of flexible filamentous particles in a rotary dryer, Exp. Thermal Fluid Sci. 44 (2013) 708–715.
[19] J. Gan, L. Chen, B. Li, W. Jiang, Y. Kitamura, A rotational drum fermentation system with water flushing for enhancing hydrolysis and acidification of solid organic wastes, Bioresour. Technol. 99 (2008) 2571–2577.
[20] E.Q. Wang, S.Z. Li, L. Tao, X. Geng, T.C. Li, Modeling of rotating drum bioreactor for anaerobic solid-state fermentation, Appl. Energy 87 (2010) 2839–2845.
[21] Y.S. Lin, W.C. Lee, K.J. Duan, Y.H. Lin, Ethanol production by simultaneous saccharification and fermentation in rotary drum reactor using thermotolerant *Kluveromyces marxianus*, Appl. Energy 105 (2013) 389–394.
[22] R.M. Rodrígues-Jasso, S.I. Mussatto, L. Sepúlveda, A.T. Agrasar, L. Pastrana, C.N. Aguilar, J.A. Teixeira, Fungal fucoidanase production by solid-state fermentation in a rotating drum bioreactor using algal biomass as substrate, Food Bioprod. Process. 91 (2013) 587–594.
[23] G.D. Dhillon, S.K. Brar, S. Kaur, M. Verma, Bioproduction and extraction optimization of citric acid from *Asperfillus niger* by rotating drum type solid-state bioreactor, Ind. Crop. Prod. 41 (2013) 78–84.
[24] F.M. Cunha, M.N. Esperança, T.C. Zangirolami, A.C. Badino, C.S. Farinas, Sequential solid-state and submerged cultivation of *Aspergillus biger* on sugarcane bagasse for the production of cellulase, Bioresour. Technol. 112 (2012) 270–274.
[25] L.W. Yoon, G.C. Ngoh, A.S.M. Chua, Simultaneous production of cellulose and reducting sugar through modification of compositional and structural characteristic of sugarcane bagasse, Enzym. Microb. Technol. 53 (2013) 250–256.
[26] Y. Huang, X. Qin, X.M. Luo, Q. Nong, Q. Yang, Z. Zhang, Y. Gao, F. Lv, Y. Chen, Z. Yu, J.L. Liu, J.X. Feng, Efficient enzymatic hydrolysis and simultaneous saccharification and fermentation of sugarcane bagasse pulp for ethanol production by cellulose from *Penicillium oxalicum* EU2106 and thermotolerant *Saccharomyces cerevisiae* ZM1-5, Biomass Bioenergy 77 (2015) 53–63.
[27] L.M. Grajales, Development of a Rotary Drum Bioreactor for Cellulolytic Enzymes Production by Solid-State Fermentation(P.h.D. Thesis) PPG-ECA/UNESP, São José do Rio Preto, 2014 (In Protuguese).
[28] D.R. Van Puyvelde, B.R. Young, M.A. Wilson, S.J. Schmidt, Experimental determination of transverse mixing kinects in a rolling drum by image analysis, Powder Technol. 106 (1999) 183–191.
[29] G.J. Finnie, N.P. Kruyt, M. Ye, C. Zeilstra, J.A.M. Kuipers, Longitudinal and transverse mixing in rotary kilns: a discrete element method approach, Chem. Eng. Sci. 60 (2005) 4083–4091.
[30] D.R. Van Puyvelde, Comparison of discrete elemental modeling to experimental data regarding mixing of solids in the transverse direction of a rotating kiln, Chem. Eng. Sci. 61 (2006) 4462–4465.
[31] A.I. Zanelato, V.M. Shiota, E. Gomes, R. da Silva, J.C. Thoméo, Endoglucanase production with the newly isolated *Myceliophthora* sp. l-1D3b in a packed bed solid state fermentor, Braz. J. Microbiol. 43 (2012) 1536–1544.
[32] F.P. Casciatori, A. Bück, J.C. Thoméo, E. Tsotsas, Two-phase and two-dimensional model describing heat and mass transfer during solid-state fermentation within a packed-bed bioreactor, Chem. Eng. J. 287 (2016) 103–116.
[33] H. Hirossue, Axial mixing of particles in rotary dryers and coolers, J. Chem. Eng. Jpn. 13 (1980) 365–371.
[34] M. Kwapinska, G. Saage, E. Tsotsas, Mixing of particles in rotary drums: a comparison of discrete element simulations with experimental results and penetration models for thermal processes, Powder Technol. 161 (2006) 69–78.
[35] E.U. Schlünder, N. Mollekopf, Vacuum contact drying of free flowing mechanically agitated particulate material, Chem. Eng. Process. Process Intensif. 18 (1984) 93–111.
[36] M.A.I. Schutyser, Mixed Solid-State Fermentation: Numerical Modeling and Experimental Validation(Ph.D. Thesis) Wageningen University, The Netherlands, 2003.
[37] S.J. Rao, S.K. Bhatia, D.V. Khakhar, Axial transport f granular solids in rotating cylinders. Part 2: experiments in a non-flow system, Powder Technol. 67 (1991) 153–162.